

SiOC(N) Cellular Structures with Dense Struts by Integrating Fused Filament Fabrication 3D Printing with Polymer-Derived Ceramics

Apoorv Kulkarni,* Joshua Pearce, Yuejiao Yang, Antonella Motta, and Gian Domenico Sorarù

Great advances have been made in various 3D printing methods for ceramics. Fabrication of Si-based ceramics using polymer-derived ceramics (PDCs) is gaining popularity. Using this route, preceramic polymers can be shaped in the polymer state and then pyrolyzed to produce different types of ceramics. Cellular ceramics can be manufactured using this technique. Herein, the novel fabrication of cellular ceramics with a two-step process using PDCs is reported. First cellular structures are 3D printed with fused filament fabrication (FFF) using thermoplastic polyurethane and impregnated with preceramic polymer polysilazane. Second, pyrolysis of the impregnated structure produces a self-similar ceramic cellular structure. The impact of 1) catalysts, 2) curing environment, and 3) pyrolysis sequence optimization to form cellular ceramics with fully dense SiOC(N) struts are systemically evaluated. The resultant custom ceramic components can tolerate operating temperatures of 1500 °C and can be manufactured for less than 5% of the cost of competing methods. The ceramic material is shown to be biocompatible and promotes fast cell adhesion. Finally, early-stage cell activation on the SiOC(N) structure is shown to be tunable by adjusting the porosity with this 3D printing to mimic the bone tissue geometry for bone regeneration.

1. Introduction

Several additive manufacturing (AM) technologies^[1–7] have been proposed for producing fully dense ceramics including selective laser sintering (SLS),^[8–10] stereolithography (SLA),^[11] laminated object manufacturing (LOM),^[12,13] binder jetting,^[14] extrusion-based printing (robocasting),^[15,16] directed energy deposition (DED),^[17] and direct ink writing (DIW).^[18]

Cellular polymer-derived ceramics (PDCs) have been proposed for applications in various fields such as catalysis,^[19] metal, liquid, and gas filtration,^[20,21] drug delivery,^[22] thermal insulation/thermal protection systems,^[23,24] and scaffolds for bone regeneration.^[25,26] Mechanical properties,^[27,28] thermal behavior,^[29] chemical and oxidation resistance^[30] for cellular ceramics has been successfully reported. Unfortunately, the use of relatively expensive AM processes has limited


access to the new opportunities for digitally manufacturing ceramic components.

AM of PDCs has been demonstrated with various methods using preceramic polymers in liquid or solid form as a feedstock combined with various AM technologies.^[31,32] SLA techniques have been showcased using liquid ceramic precursors such as polysiloxanes, polysilazanes, and polycarbosilanes. To make the preceramic polymers compatible with the SLA process, they must be chemically modified to add photosensitive functionalities or combined with photosensitive resins.^[33,34] In this latter case, careful control over the composition of the chemical mixture is required to obtain optimum rheological and optical attributes.^[35] Binder jetting-type AM has also been used with solid preceramic polymer powders as the feedstock of the process. The powders are then bound layer by layer using a binder solution.^[36] The binder solution has to be optimized to have a suitable rheology and concentration of polymer binders and crosslinking agents for the preceramic polymers.^[37] DIW, which can be considered a subtype of fused filament fabrication (FFF) printing, uses preceramic polymers combined with solvents to obtain the optimum rheology for 3D printing.^[38,39] Ceramic composites can also be manufactured using DIW by including additives in the ink solution. Ceramic structures were obtained by adding

A. Kulkarni, G. D. Sorarù
Glass & Ceramics Lab, Department of Industrial Engineering
University of Trento
Via sommarive 9, Povo 38123, Trento, Italy
E-mail: apoorv.kulkarni@unitn.it

J. Pearce
Thompson Centre of Engineering Leadership & Innovation
Department of Electrical and Computer Engineering
Western University
Thompson Engineering Building, 1151 Richmond St. N., London, ON N6A
5B9, Canada

Y. Yang, A. Motta
BIOTech, Center for Biomedical Technologies, Department of Industrial
Engineering
University of Trento
Via Sommarive 9, Povo 38123, Trento, Italy

 The ORCID identification number(s) for the author(s) of this article can be found under <https://doi.org/10.1002/adem.202100535>.

© 2021 The Authors. Advanced Engineering Materials published by Wiley-VCH GmbH. This is an open access article under the terms of the Creative Commons Attribution License, which permits use, distribution and reproduction in any medium, provided the original work is properly cited.

DOI: 10.1002/adem.202100535

boron nitride powder to polysilazane ink solution to achieve superior mechanical properties.^[40] Similarly, ceramic composites were obtained by adding silicon carbide powder and carbon fiber chops to the polysiloxane ink solution.^[41] A novel method is also described where a solution of polysiloxane preceramic polymer was printed in a support bath/gel made from mixing fumed silica and mineral oil. The rheological properties of both the support gel and the printing solution have to be controlled and optimized to have decent printability.^[42] A method similar to the one proposed in this article was reported by some of the authors using FFF 3D printing, where 3D printed structures were coated with polysiloxane preceramic to obtain hierarchically porous cellular ceramics.^[43] SLS using preceramic polymers was also successfully showcased where polysiloxane powder mixed with SiC filler was selectively cured and pyrolyzed using laser sintering.^[44]

The aforementioned processes, however, are limited by some inherent challenges. Such as in SLA, even though very good resolution can be obtained, the resin has to be chemically modified to obtain the suitable rheological and optical properties. Also, the process has to be conducted under controlled environment to avoid crosslinking of the liquid resin and to avoid the toxic fumes from releasing into the environment. With DIW, the rheology of the inks has to be maintained to achieve good printability. The method also lacks in resolution compared with other processes due to the same reason. Similar consideration to the binders in the binder jetting process has to be given to maintain printability. Parts made from binder jetting contain porosity as the process starts from powders and the sintering postprocessing does not close all the porosities in the ceramic parts. The process also has to be conducted in a controlled environment as the micrometer-sized powders can be a health hazard.

FFF is the most accessible and widespread method of AM, which was made possible by the open source release of the self-replicating rapid prototyper (RepRap) project.^[45] Yet, there is a lack of research in the area of integrating FFF 3D printing with PDCs. This study aims to fill the gap using PDCs with the low cost and simple process control of the FFF 3D printing method to produce cellular ceramics with dense struts.^[46–48] The method uses similar approach of replicating acrylic lattice 3D printed with SLA.^[49]

The proposed method uses a two-step process, first to 3D print cellular structures with FFF 3D printing using thermoplastic polyurethane (TPU)-based filaments and impregnating the structure with preceramic polymer (polysilazane). Second, pyrolysis of the impregnated structure produces a self-similar ceramic cellular structure. The method successfully attempts to overcome the drawbacks of previously mentioned AM methods using preceramic polymers using low-cost FFF open source 3D printing. As the method uses a desktop 3D printer with commercially available filaments, the printing process does not need to be conducted under a controlled environment unlike SLA and binder jetting. The method also uses commercially available preceramic polymers and solvents which do not require any chemical modification to be suitable for the process. Usage of commercially available polymer filament also avoids production of rheologically controlled ink unlike DIW process. The method also utilizes less power compare with the high-power laser used in SLS.

This study systemically evaluates the impact of 1) catalysts, 2) curing environment, and 3) pyrolysis sequence optimization

to form cellular ceramics with fully dense SiOC(N) struts via the combination of FFF-based 3D printing with polysilazane-based PDCs. The resultant materials are quantified by hardness depth profiles and compressive strength of completed parts. The results are discussed in the context of three applications that are demonstrated with low-cost ceramic components for medical, aerospace, and high temperature systems.

2. Experiments

The initial tests were done using TPU filaments with varying shore hardness; Matterhackers Pro TPU (90A), Matterhackers TPE (98A), Ninjatek NinjaFlex (85A) Fillamentum Flexfill (98A), and Colorfabb nGen Flex (95A). The samples were printed as cellular structures with 1.2 mm² cells. The samples were then impregnated with the preceramic polymer (durazane) solution and then pyrolyzed at 1200 °C to obtain the final ceramic (see Experimental Section).

The 1.2 mm cell size forms a vertical channel, which creates a capillary structure for the preceramic polymer solution to rise through the channels. This in turn reduces the necessity to have the excess amount of solution to totally submerge the sample, nearly eliminating chemical waste.

Characterization of the TPU filaments with differential scanning calorimetry (DSC) (Figure 1) reveals that the lower the shore hardness the lower the glass transition temperature (T_g). T_g represents the glass transition of the soft segments.^[50] The T_g ranges from -52.5 °C (Ninjaflex 85A) to -13.7 °C (PRO TPE 98A). The glass transition temperature is affected by many factors. Lower T_g indicates higher amounts of amorphous phase in the semicrystalline polymer. T_g also depends on length of the

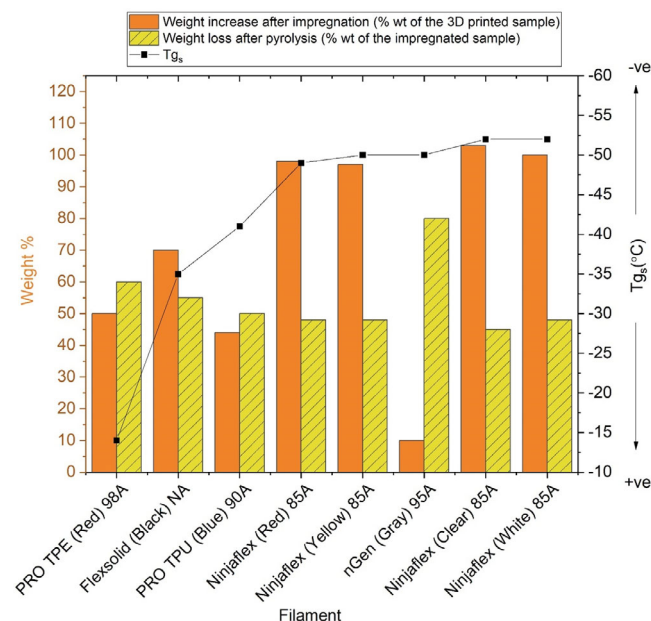


Figure 1. Comparison of TPU filaments of different shore hardness with their glass transition temperatures (T_g) with increase in weight after impregnation with the preceramic polymer and weight loss after the pyrolysis.

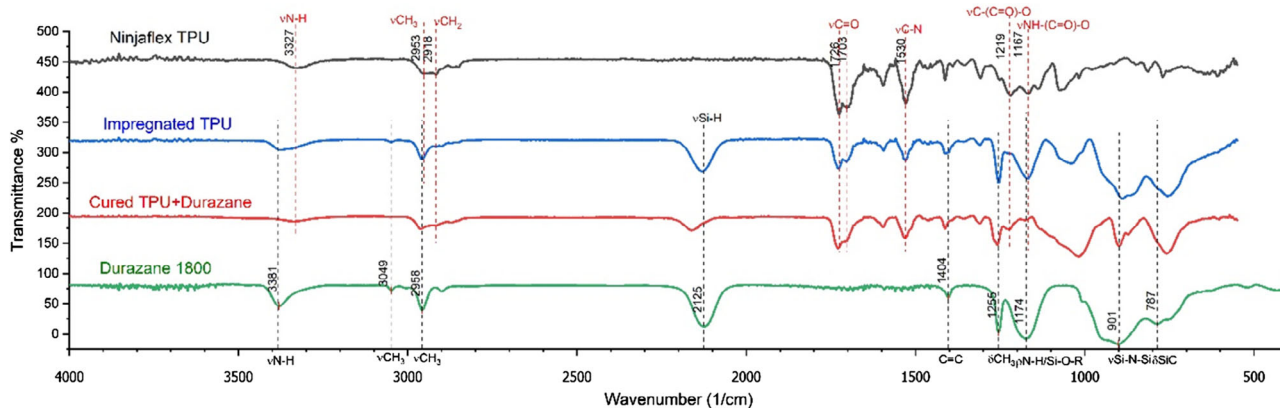


Figure 2. Comparison of FTIR spectra of i) Ninjaflex TPU filament; ii) TPU filament impregnated with durazane precursor; iii) impregnated filament cured at 160 °C for 3 h; and iv) Pure Durazane 1800 precursor.

linear polymer chains. The lower the T_g , the greater the length of the chain, which gives the polymer more flexibility.^[51] Finally, T_g can also depend on the additives put into the commercial filaments to give them their specific properties such the surface texture and color. The impregnation tests also showed that the more flexible the TPU filament the higher the amount of preceramic polymer retained and, subsequently, the higher the final ceramic yield (Figure 1).

The clear Ninjaflex TPU filament presented the best results regarding the weight increase and final ceramic yield. Weight increase of $100 \pm 5\%$ after impregnation, $65 \pm 5\%$ volume increase, and $17.5 \pm 2.5\%$ increase in linear dimensions were noted after the impregnation indicating successful diffusion and interaction between TPU and polysilazane.

As the 3D printed part after impregnation contains both TPU and durazane in the same amount, the thermal behavior of the TPU filament as well as durazane precursor must be considered. The DSC analysis of the NinjaFlex TPU filament shows that it starts melting around 165 °C. The DTA analysis of the liquid polysilazane precursor mixed with Pt catalyst ($100 \mu\text{L g}^{-1}$ precursor) with constant heating rate of $10^\circ\text{C min}^{-1}$ in nitrogen atmosphere, shows an exothermic peak at 250 °C suggesting that that it crosslinks into a thermoset polymer around this temperature. This means that, at a constant heating rate, the impregnated PU part will melt and lose its structure before the crosslinking of the durazane. This implies that a modified heat treatment is necessary for the polysilazane to be crosslinked before the TPU filament reaches the melting onset. According to recent studies,^[52] polysilazanes can be crosslinked at lower temperatures in air atmosphere. The moisture in air helps to activate the crosslinking at temperatures as low as 120 °C when exposed for long times by promoting hydrolysis and polycondensation reactions. Following the modified heat treatment schedule, with the isothermal curing at 160 °C, the 3D-printed structures were successfully pyrolyzed into self-similar ceramic structures.

Weight loss of $50 \pm 2\%$ was observed during the polymer to ceramic transformation. The ceramic yield from pure durazane is reported to be 65–70%. The Ninjaflex filament decomposes up to 95% above 500 °C. If there was no interaction between the TPU and the polysilazane, expected ceramic yield of the system

would be only 35–40%. The 50% final yield from the NinjaFlex and durazane system indicates the existence of some chemical reaction forming intermediate products, which contribute to the extra 10% ceramic yield.

Further investigations with the FTIR (Figure 2) show that, in the cured sample, the Si–H peak coming from the polysilazane is shifted toward higher wavenumber and the $-\text{NH}-(\text{C}=\text{O})-\text{O}$ (urethane) peak disappears after crosslinking. N–H peak at 3380 cm^{-1} coming from durazane are reduced after crosslinking. Taken all together, this information indicates that there might be some chemical interaction occurring between the TPU polymer and the polysilazane, which further promotes the impregnation and increases the ceramic yield.

The scanning electron microscope (SEM) images (Figure 3a,c) show that the struts are completely dense, indicating that the impregnation was successful.

The elements' profiles (Figure 3b) demonstrate that Si is present in high amount even at $140 \mu\text{m}$ beneath the surface, which means at the center of the struts (thickness around $280\text{--}300 \mu\text{m}$). This is the result of durazane easily diffusing in the TPU structure. Indeed, a similar energy dispersive spectroscopy (EDS) study conducted on the impregnated TPU component (see Supporting Information) confirmed the presence of Si through the strut cross section and, also, evidenced a localized higher concentration of Si at the surface of the struts, which should be related to the deposition of a thin durazane coating.

Moreover, the SEM (Figure 3a) shows some bright regions near the surface of the struts and the EDS scan of the cross section (Figure 3b) reveals a Si gradient in the first $60 \mu\text{m}$ with a higher concentration close to the surface. The reason can be that, together with the diffusion of polysilazane in the PU structure, also a thin layer of polysilazane can deposit on the surface of the struts explaining the formation of the bright, Si-rich, regions.

The easy diffusion of durazane into the TPU structure is probably due to a good chemical affinity between the two polymers which have similar functional groups (N–H and urethane groups), unlike the polysiloxane which has less chemical similarity with the TPU and the impregnation process results into a thin coating on the surface of the surface compared with the diffusion

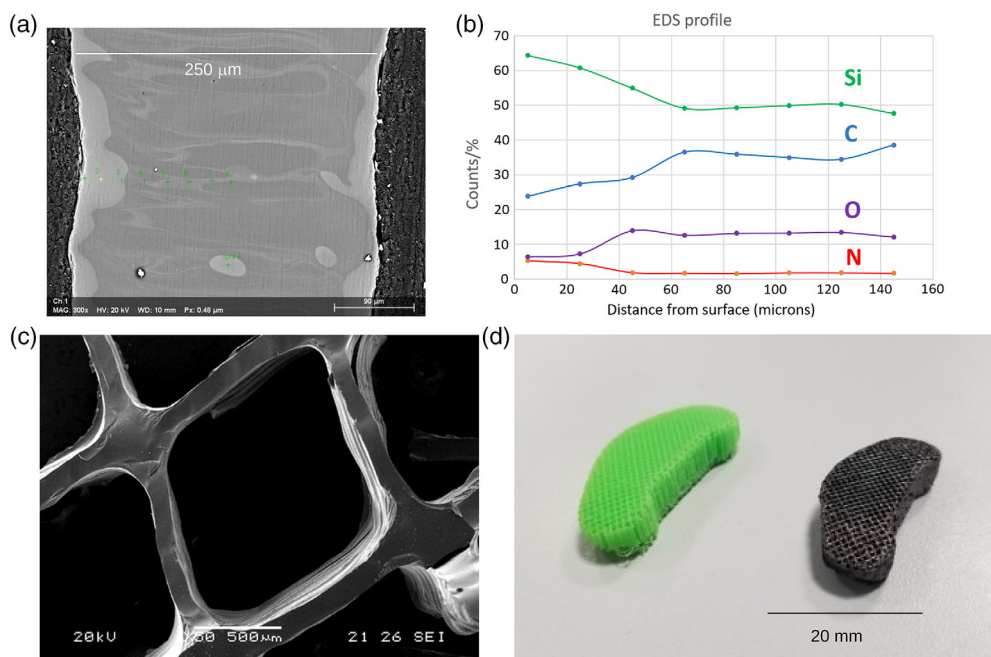


Figure 3. a) Backscatter image of cross section of the strut of the final ceramic component with points for EDS analysis. b) EDS profiles of Si, C, O, and N going from the surface to the center. c) SEM image of the fracture surface of the ceramic sample. d) 3D-printed prototype spinal disc for potential prosthetic use in human spine and the converted ceramic counterpart. Note: the EDS profile is not quantitative but provides a qualitative view on the change in composition of elements from the surface to the core.

to the core. This leads a formation of hollow ceramic struts instead of a fully dense strut.^[43]

The carbon and oxygen profiles (Figure 3b) show an increase toward the center of the struts. The oxygen presence cannot be attributed to the oxidation occurring during the curing process in air. Indeed, if this was the case then a reverse oxygen profile, with higher concentration near the surface and decreasing toward the core would have been found. Most probably oxygen comes from a reaction between the decomposing urethane groups, producing CO_2 ^[53] and the polysilazane. Such reaction would also explain why the amount of nitrogen measured was low compared with the expected silicon carbonitride (SiCN) ceramic composition from polysilazane precursors.^[54] Indeed, it is known that pyrolysis of polysiloxanes in CO_2 flow results in cleaving the Si–C bonds and formation of new Si–O bonds.^[55,56] Thus, it can be tentatively assumed that a similar reaction occurs between the in situ produced CO_2 and Si–N bonds of polysilazane, resulting into an increase in oxygen in the ceramic residue and an elimination of nitrogen as N_2 or NH_3 .

3. Testing

Chemical analysis shows the average composition of the ceramic samples. Nitrogen was observed to be no more than 2 mass%. The average phases of the ceramic were calculated as (mass%) 56% SiO_2 , 4.3% Si_3N_4 , 9.2% SiC, and 30.5% free carbon making the final composition $\text{SiO}_{1.5}\text{C}_{0.18}\text{N}_{0.1} + 2 \text{C}_{\text{free}}$.

The density of the material was found to be 2.12 g cm^{-3} , which is similar to SiOC ceramics reported in the literature.^[57] The hardness of the silicon- and nitrogen-rich surface region was

found to be $8.6 \pm 0.5 \text{ GPa}$ and that of the oxygen + carbon-rich core regions were found to be $7.1 \pm 0.2 \text{ GPa}$.

Compression samples with dimensions $20 \times 20 \times 10 \text{ mm}^3$ (see Supporting Information) were tested with two different types of infill grid and trihexagonal with 1.2 mm cell size (25% infill density). The infill pattern was exposed along the direction of the load. The average compressive strength for trihexagonal infill was $24 \pm 1.5 \text{ MPa}$, whereas for grid-type samples was $22 \pm 1.8 \text{ MPa}$.

Samples with dimensions $45 \times 6 \times 3 \text{ mm}^3$ (see Supporting Information) for four-point bending tests were printed with 25% dense grid and trihexagonal infill, with the infill pattern perpendicular to the direction of the load. The average flexural strength of the grid infill samples was $17 \pm 3 \text{ MPa}$, and for trihexagonal infill, it was $18 \pm 0.7 \text{ MPa}$.

One of the main areas where silicon-based ceramics can be utilized are high temperature applications. Taking advantage of the PDC route ultrahigh temperature-resistant ceramic materials can be obtained.^[58] Silicon-based PDCs, for example, can be high temperature-resistant for temperatures greater than 1000°C .^[59] Cellular ceramics are beneficial in many fields as they possess better thermal and physical properties than the bulk ceramics in some cases.^[60] Open cell ceramic structures also possess better thermal conductivity as heat transfer is improved because of the fluid flow through the cells.^[61] Silicon-based ceramics have a higher specific heat capacity compared with alumina and zirconia as well as higher thermal conductivity and thermal shock resistance. Therefore, silicon-based cellular ceramics can find applications in fields as porous burners and high temperature catalyst carriers.^[62] For applications such as

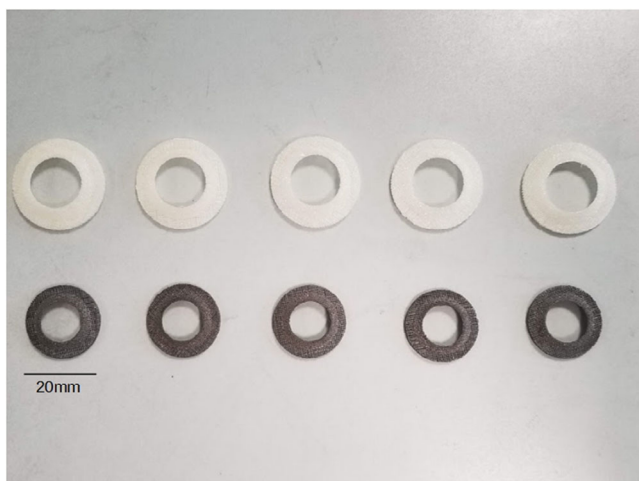


Figure 4. Ring-shaped spacer parts to test the fitting tolerances.

heat shields and heat exchangers, the ceramic parts need to fit industrial tolerances.^[63]

To check the fitting tolerances, a ring-shaped part to fit between two metal plates (**Figure 4**) was designed with final dimension requirements of 20 mm outer diameter, 15 mm inner diameter, and 4 mm thickness. As from the previous experiments, the average increase in linear dimensions was 17.5% during impregnation and the average decrease after pyrolysis was 32%. The parts were printed with the dimensions of 25 mm diameter and 5 mm thickness. These measurements were then increased to 29.3 ± 0.1 mm in diameter and 5.9 ± 0.1 mm in thickness. After the pyrolysis, the standard deviation in the diameter measurement was 0.11 with the mean being 19.87 mm, and for the thickness measurement, standard deviation and mean being 0.05 and 4.01 mm, respectively. The mechanical tolerance of the parts was within 0.1 mm, which is the limit set by the FFF printer used.

4. Testing for Applications

4.1. High Temperature Applications

The same samples were used for high temperature stability testing. After 12 h at 1500 °C, $0.5 \pm 0.15\%$ weight loss and $2 \pm 0.25\%$

shrinkage in the linear dimensions was observed with a reflective layer formed on the structure. This suggests that the structure is not losing mass, which might affect the performance at high temperatures. The reflective layer can be a result of the oxidation and formation of a thin, passivating, silica layer. SEM pictures of the ceramic components before and after the oxidation are shown in **Figure 5**. The component after oxidation for 12 h at 1500 °C in air does not show any major modification. To get more insights into the oxidation behavior a TGA was carried out in flowing air up to 1500 °C (see Supporting Information). This experiment showed the presence of only one weight loss step between 600 and 1200 °C of ≈ 2 wt% which can be attributed to the oxidation of free carbon. The 0.5 wt% loss measured in the bulk samples after the oxidation in air for 12 h must therefore be the results of the 2 wt% weight loss due to C oxidation and an opposite weight increase due to the formation of a silica scale.

Other oxidation studies done on polymer-derived SiOC ceramics show that the system undergoes passive oxidation as the activity of the free carbon present in the ceramic is very low.^[64] The outer layer being rich in silicon and nitrogen as well as most of the free carbon being in the center of the strut might help preventing the oxidation of the free carbon. Previous research also shows that SiOC (N) ceramics exhibit a higher thermal stability due to inclusion of nitrogen.^[65,66]

4.2. Scaffoldings for Bone Tissue Regeneration

One of the main applications for which the cellular ceramic can be used is scaffoldings for bone regeneration.^[67,68] Ceramic AM with materials like hydroxyapatite, bioactive glasses, polylactic acid, zirconia, and calcium phosphate has already been demonstrated.^[26,69] Moreover, SiOC ceramic nanowires in the form of scaffoldings have already been tested for biocompatibility. SiOC ceramic structures have been shown not to be cytotoxic and to support cell growth and activity beneficial for tissue regeneration.^[70] SiOC material has also been tested for blood contact applications resulting in good hemocompatibility due to the presence of pyrolytic carbon.^[71] Similarly, the 3D-printed ceramic scaffoldings need to satisfy the cytotoxicity and cell proliferation tests as a first step to be considered compatible as scaffoldings for bone tissue regeneration.^[72]

Figure 6a shows the results of the cytotoxicity test for the high density (200 μm) and low density (500 μm) samples. The cell death ratios after 24 and 48 h are close to the negative control

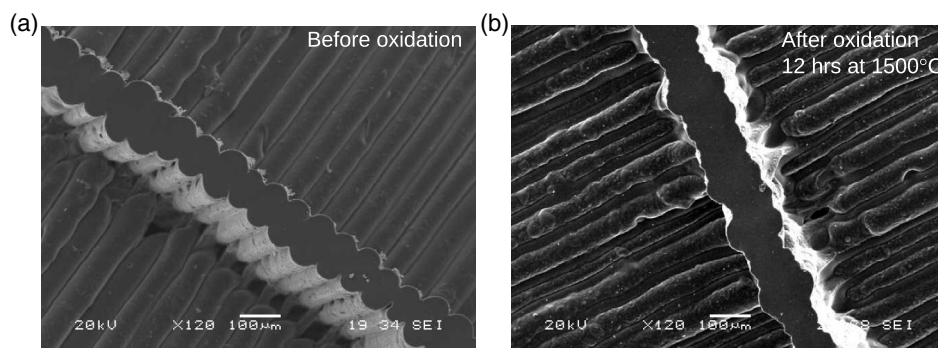


Figure 5. SEM image of the fracture surface of the ceramic a) before oxidation and b) after oxidation on the left.

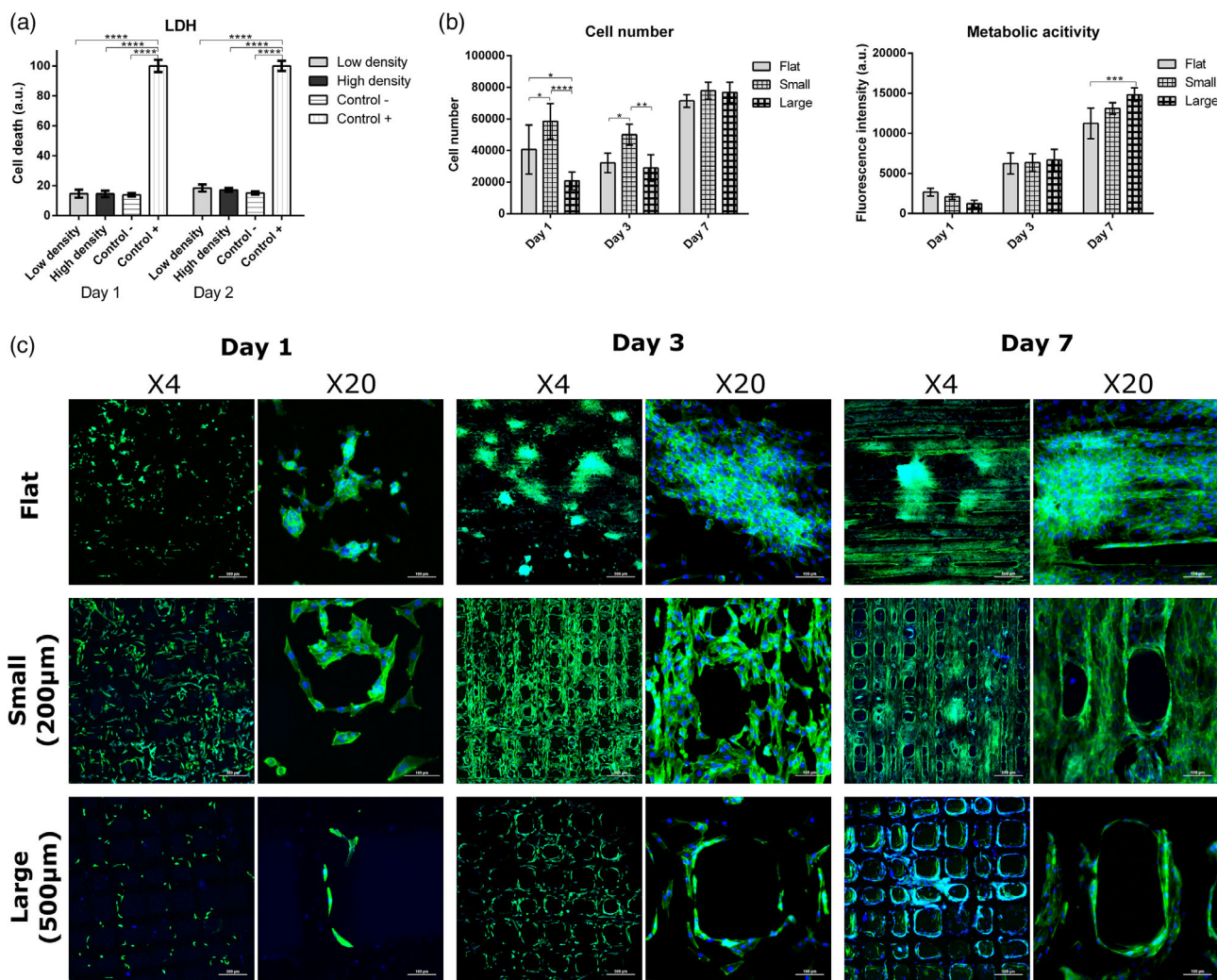


Figure 6. a) Cell death ratios on low density (500 μm pores) and high density (200 μm pores) samples compared with the negative control sample. b) Increase in cell number and cell metabolic activity on flat, small pore, large pore samples on day 1, day 3, and day 7. c) Confocal images of cell growth on flat, 200 μm pore and 500 μm pore samples after day 1, day 3, and day 7.

samples, indicating the materials are not cytotoxic, and the infill density does not affect the cytotoxicity. Figure 6b shows that from day 1 to 7, the total cellular metabolic activity increased gradually in general; however, samples with larger porosity showed the highest activation if compared with the reference system, flat sample. Figure 6c shows the results of cell adhesion, metabolism, and proliferation. The cells seemed to proliferate when cultured with smaller porosity, however, they grew in a monolayer on the top surface bridging the pores. The lower-density samples with 400 μm pores seemed to help the cell adhesion and together cell migration growth inside the pores, instead of forming the surface layer, but with a slower proliferation rate. In all the samples, the cell-to-cell connections are clearly visible.

5. Cost Calculation

The main concern when it comes to specialized materials and custom applications is the cost. Even if AM saves costs in

inventory, assembly, retailing, and distribution compared with the conventional manufacturing processes, AM methods such as laser sintering and thermal jetting have high capital and operating costs associated to them. This study has shown that the distributed manufacturing model using low-cost FFF-based 3D printing, which has proven to consistently reduce costs fabricating open source designs,^[73] also reduces the materials costs of custom ceramic components to less than 5% of those currently commercially available.

The machine costs for SLS printers constitute almost 60% of the total production costs over its lifetime, with the machines costing around \$500 000.^[74] The cost of energy consumption for laser-based systems can be as high as 500% compared with the FFF 3D printing,^[75] which have been shown to be even less energy intensive than conventional manufacturing when used for distributed manufacturing.^[76] This energy efficiency in production also reflects in the cost of the commercial product when one needs to get a part printed from a company.

Table 1. Cost analysis of manufacturing 1 component and 10 components.

Consumables	Cost	Spinal disc (150 μm nozzle)	Cost (Euros)	Spinal disc (10 pieces)	Cost (Euros)	Nozzle (250 μm nozzle)	Cost (Euros)	Nozzle (10 pieces)	Cost (Euros)
Electricity for printer (500 W)	€0.25 kWh ⁻¹	25 min (0.208 kWh)	0.05	17 h (8.5 kWh)	2.125	3 h 54 min (2 kWh)	0.5	39 h 18 min (20 kWh)	5
TPU filament	€40/750 g	0.001 g	0.01	92 g	5	9 g	0.53	98 g	5.24
Durazane	€200/1 kg	10 g	2	100 g	20	30 g	6	300 g	60
Pt catalyst	€150/5 mL	25 μL	0.75	250	7.5 μL	75 μL	2.25	750 μL	22.5
Acetone	€50 L ⁻¹	10 mL	0.5	100 mL	5	30 mL	1.5	300 mL	15
<i>p</i> -Xylene	€100 L ⁻¹	475 μL	0.04	4.75 mL	0.4	1.425 mL	0.12	14.25 mL	1.2
Electricity for furnace (7500 W)	€0.25 kWh ⁻¹	6.16 h (46.25 kWh)	11.5	6.16 h (46.25 kWh)	11.5	6.16 h (46.25 kWh)	11.5	6.16 h (46.25 kWh)	11.5
Nitrogen (300 cc/min for 9 h)	€110/(8 L 150 bar)	162 L	15	162 L	15	162 L	15	162 L	15
Total cost			29.85		66.525		37.4		135.44
Cost per piece					6.6525				13.54

Table 2. Cost comparison of commercial ceramic AM and FFF 3DP.

	AM method	Spinal disc 1 piece (Euros)	Spinal disc batch (Euros)	Nozzle 1 piece (Euros)	Nozzle batch (Euros)
Steinbach AG (alumina)	SLA	745	220/piece (for 10 pieces)	1900	1145/piece (for 5 pieces)
Creutz 3D (alumina)	SLA	780	282/piece (for 5 pieces)	780	282/piece (for 5 pieces)
Creutz 3D (zirconia)	SLA	1380	584/piece (for 5 pieces)	1380	584/piece (for 5 pieces)
Formatec (silica)	Digital light processing	Cannot make.	Cannot make.	950	NA
Protiq marketplace (alumina)	SLA	1927	NA	3117	NA
UniTrento	TPU replica	29.85	6.6525/piece (for 10 pieces)	37.4	13.544/piece (for pieces)

To compare the production costs, quotes were obtained from commercial manufacturers of ceramic 3D printed parts for a spinal disc (bioceramic part) and a microsatellite nozzle (high temperature application part) (Figure S2, Supporting Information) with the materials that would satisfy the application requirements. A simple model to analyze the production cost of the parts with this method was used.^[77] The cost of the build can be calculated as

$$C_{\text{build}} = (C_{\text{energy}} \times T_{\text{build}})_{\text{printer}} + (M \times P_{\text{raw material}}) + (C_{\text{indirect}} \times T_{\text{pyrolysis}}) \quad (1)$$

where

C_{energy} = cost of energy consumption for the printer per hour; T_{build} = time for the build; M = amount of raw material used (this consists of the TPU filament, Durazane 1800, Acetone solvent, Pt Catalyst, *p*-xylene solvent); $P_{\text{raw material}}$ = price of the raw material; C_{indirect} = indirect costs for the furnace (this consists of the energy consumption, the purging gas, and the cooling water); $T_{\text{pyrolysis}}$ = time the furnace is operated for the pyrolysis.

Table 1 shows the costs estimation for a single part and a batch of 10 parts.

The nozzle is also manufactured as a cellular structure with the impregnation method as it provides more surface area for better heat dissipation without losing any functionality as a heat shielding component.

Table 2 shows the material costs for the parts from commercial ceramic AM companies. It shows that the distributed manufacturing ceramics with the impregnation approach reduces the cost by as much as 200–300%.

6. Conclusion

In conclusion, it has been demonstrated for the first time, that SiOC (N) cellular ceramic structures with fully dense struts can be manufactured by impregnating preceramic polymers into FFF 3D-printed TPU structures in fraction of the cost of the competing methods.

With the use of an open source 3D printing technique, the principal cost of investing in expensive machinery is saved.^[78] The method uses commercially available materials, which brings the operating costs down. The same part can be manufactured at 5% of the material cost compared with the commercial manufacturers using a distributed manufacturing technique.

The novel method demonstrated in the research eliminates the possibility of having pores with complete impregnation of

the preceramic polymer in the TPU structure, which can be manufactured with industrial tolerances. The material of the ceramic is biocompatible and promotes fast cell adhesion, and early stage cell activations, which gives the possibility to mimic the bone tissue geometry for bone regeneration.

In the future, the method can be modified to manufacture ceramic composites by either adding nanofillers in the preceramic polymer solution or modifying the TPU filament to expand the use of the structures in applications such as active filters, catalytic converters, or electrically conductive applications.

7. Experimental Section

FFF Printing: The filaments were printed on an open source Lulzbot TAZ 6 (Fargo Additive Manufacturing Equipment 3D, LLC, USA) with nozzles of size 0.15 and 0.25 mm.

Design of Samples: The samples were designed as $20 \times 20 \times 10$ mm³ cubes using OpenSCAD 2015.03 and prepared as cellular structures with line-type infill and line distance (cell size) of 1.2 mm using the open source Lulzbot Cura 3.6.21 slicer.

Impregnation: A commercial polysilazane (Durazane 1800; CAS: 503590-70-3; Merck, Darmstadt, Germany), precursor for SiCN ceramic, was used along with the catalyst platinum divinyltetramethyldisiloxane complex, \approx Pt 2% in xylene (CAS number: 68478-92-2, Sigma-Aldrich, St. Louis, MO, USA) diluted to 0.1%. Pt catalyst promoted the crosslinking of the preceramic polymer via hydrosilylation reaction between the Si-H and the C=C moieties present in the silicon polymer.^[79] The TPU sample was first submerged in a solution of 5 g acetone and 500 μ L of catalyst. After 15 min, 5 g of the preceramic polymer was added and kept for 4 h changing sides after 2 h. The samples were then taken out and dried for 24 h in air at room temperature.

Heat Treatment: The samples were then treated in an alumina tube furnace (GERO tube furnace) at 160 °C (10 °C min⁻¹) in air flow (400 cc min⁻¹) for 3 h and then free cooling back to room temperature. The furnace was then purged with nitrogen flow (400 cc min⁻¹) for 2 h following a pyrolysis to 1200 °C with 1 h dwelling at the maximum temperature. The samples were then cooled to room temperature at 10 °C min⁻¹. For biological evaluations, the samples were rinsed by deionized water (DI water) and then sterilized by autoclave at 121 °C for 15 min.

Characterization of TPU Filaments: For the characterization of the TPU filaments for their thermal behavior, DSC (Mettler DSC30) and infrared spectroscopy (ATR, Varian 4100 FTIR, Agilent Technologies Inc., USA) were carried out. Fourier transform infrared spectroscopy was also done on the as received Durazane 1800 (Nicolet Avatar 330 FTIR spectrometer, Thermo Fisher Scientific, Waltham, MA, USA).

The crosslinking of the preceramic polymer and decomposition of TPU filaments was examined using simultaneous differential thermal analysis (DTA) and thermogravimetric analysis (TGA) (Netzsch STA 409 Netzsch GmbH, Selb, Germany) at 10 °C min⁻¹ up to 1200 °C in flowing Air/N₂ (150 cc min⁻¹).

Mechanical Testing: Density of the final ceramic is measured with a helium pycnometer (AccuPyc 1330TC, Micromeritics, Norcross, GA, USA). Hardness testing was also done along polished section of the struts with FM-310 microhardness tester (Future Tech). Compression tests and four-point bending tests were carried out using Instron 5969 testing machine with 10 kN load cell with displacement 1 mm min⁻¹.

Electron Microscopy and EDS: The ceramic morphology and elemental composition from the surface to center of the struts were characterized using EDS with scanning electron microscope Jeol JSM-IT300LV.

High Temperature Stability: To check the high temperature stability, the samples were held in air for 12 h at 1500 °C and the weight and dimension changes were observed.

Biocompatibility for Scaffoldings as Bone Tissue Regeneration: The samples were also tested for biocompatibility for the purpose of regeneration

of bone tissue. The samples were designed as discs of diameter 13 mm and thickness 1.5 mm with pore sizes of 200 and 500 μ m.

The cytotoxicity was evaluated on sample extracts using the lactate dehydrogenase assay (LDH assay-TOX-7 Sigma) on NIH 3T3 cell lines (murine embryo fibroblast, ATCC) in vitro cultures, by following ISO 10993-5 protocol with experimental time points on days 1 and 2 against a control group of cells cultured in the standard medium.

The cell behavior on porous samples was evaluated by culturing MG63 (human osteosarcoma, ATCC) cells up to 7 days and measurements were done on day 1, 3, and 7.

To evaluate the cell proliferation PicoGreen DNA quantification assay (Quant-iT PicoGreen dsDNA Assay, Invitrogen, Carlsbad, USA) was used. For both the cell behavior and the cell proliferation tests, flat samples of the same material were used as control and measurements were taken after day 1, 3, and 7.

Cell metabolic activity was determined by AlamarBlue Cell Viability assay (Invitrogen, Carlsbad, USA), that quantifies cellular metabolic activity and in turn determines the concentration of viable cells in each sample. Measurements were taken after day 1, 3, and 7. Cell morphology and distribution were visualized by Oregon green phalloidin (cytoskeleton filament) and 4'6-diamidino-2-phenylindole (DAPI) (nuclei) staining and observed using Zeiss LSM 510 Meta confocal laser scanning microscope.

Supporting Information

Supporting Information is available from the Wiley Online Library or from the author.

Acknowledgements

G.D.S., A.K., and A.M. acknowledge the financial support by the Italian Ministry of University and Research (MIUR) Department of Excellence 2018–2022 (DII-UNITN-Regenera project). The authors thank Aleph Objects for providing with the printer hardware.

Conflict of Interest

The authors declare no conflict of interest.

Data Availability Statement

Data available on request from the authors.

Keywords

Additive manufacturing, Fused filament fabrication, Open source 3D printing, Polymer-derived ceramics, Polysilazanes, preceramic polymers, Thermoplastic polyurethanes

Received: May 3, 2021

Revised: July 2, 2021

Published online:

- [1] L. C. Hwa, S. Rajoo, A. M. Noor, N. Ahmad, M. B. Uday, *Curr. Opin. Solid State Mater. Sci.* **2017**, *21*, 323.
- [2] T. D. Ngo, A. Kashani, G. Imbalzano, K. T. Q. Nguyen, D. Hui, *Compos. Part B Eng.* **2018**, *143*, 172.
- [3] P. Colombo, G. Mera, R. Riedel, G. D. Sorarù, *J. Am. Ceram. Soc.* **2010**, *93*, 1805.
- [4] P. Greil, *Adv. Eng. Mater.* **2000**, *2*, 339.

- [5] R. Riedel, G. Mera, R. Hauser, A. Klönczynski, *J. Ceram. Soc. Jpn.* **2006**, *114*, 425.
- [6] J. Zeschky, F. Goetz-Neunhoeffler, J. Neubauer, S. H. Jason Lo, B. Kummer, M. Scheffler, P. Greil, *Compos. Sci. Technol.* **2003**, *63*, 2361.
- [7] C. Vakifahmetoglu, D. Zeydanli, P. Colombo, *Mater. Sci. Eng. R Rep.* **2016**, *106*, 1.
- [8] D. L. Bourell, H. L. Marcus, J. W. Barlow, J. J. Beaman, *Int. J. Powder Metall. Princet. N. J.* **1992**, *28*, 369.
- [9] Ph. Bertrand, F. Bayle, C. Combe, P. Goeuriot, I. Smurov, *Appl. Surf. Sci.* **2007**, *254*, 989.
- [10] B. Qian, Z. Shen, *J. Asian Ceram. Soc.* **2013**, *1*, 315.
- [11] J. W. Halloran, *Annu. Rev. Mater. Res.* **2016**, *46*, 19.
- [12] H. Windsheimer, N. Travitzky, A. Hofenauer, P. Greil, *Adv. Mater.* **2007**, *19*, 4515.
- [13] L. Weisensel, N. Travitzky, H. Sieber, P. Greil, *Adv. Eng. Mater.* **2004**, *6*, 899.
- [14] J. Moon, J. E. Grau, V. Knezevic, M. J. Cima, E. M. Sachs, *J. Am. Ceram. Soc.* **2002**, *85*, 755.
- [15] X. Lu, Y. Lee, S. Yang, Y. Hao, J. R. G. Evans, C. G. Parini, *J. Eur. Ceram. Soc.* **2010**, *30*, 1.
- [16] E. Feilden, E. G.-T. Blanca, F. Giuliani, E. Saiz, L. Vandeperre, *J. Eur. Ceram. Soc.* **2016**, *36*, 2525.
- [17] R. Banerjee, P. C. Collins, A. Genç, H. L. Fraser, *Mater. Sci. Eng. A* **2003**, *358*, 343.
- [18] Direct Ink Writing of Three-Dimensional Ceramic Structures - Lewis - 2006 - Journal of the American Ceramic Society - Wiley Online Library, <https://ceramics.onlinelibrary.wiley.com/doi/full/10.1111/j.1551-2916.2006.01382.x>.
- [19] T. Konegger, L. F. Williams, R. K. Bordia, *J. Am. Ceram. Soc.* **2015**, *98*, 3047.
- [20] M. C. Bruzzoniti, M. Appendini, L. Rivoira, B. Onida, M. D. Bubba, P. Jana, G. D. Sorarù, *J. Am. Ceram. Soc.* **2018**, *101*, 821.
- [21] J. Adler, *Int. J. Appl. Ceram. Technol.* **2005**, *2*, 429.
- [22] C. Vakifahmetoglu, D. Zeydanli, V. C. Ozalp, B. A. Borsa, G. D. Sorarù, *Mater. Des.* **2018**, *140*, 37.
- [23] M. Zhu, R. Ji, Z. Li, H. Wang, L. Liu, Z. Zhang, *Constr. Build. Mater.* **2016**, *112*, 398.
- [24] C. Xu, S. Wang, K. Flodström, X. Mao, J. Guo, *Ceram. Int.* **2010**, *36*, 923.
- [25] H. Ma, C. Feng, J. Chang, C. Wu, *Acta Biomater.* **2018**, *79*, 37.
- [26] G. Brunello, S. Sivoletta, R. Meneghello, L. Ferroni, C. Gardin, A. Piattelli, B. Zavan, E. Bressan, *Biotechnol. Adv.* **2016**, *34*, 740.
- [27] S. Meille, M. Lombardi, J. Chevalier, L. Montanaro, *J. Eur. Ceram. Soc.* **2012**, *32*, 3959.
- [28] D. J. Green, in *Proc. Metallurgical Society of the Canadian Institute of Mining and Metallurgy* (Eds.: W. R. Tyson, B. Mukherjee), Pergamon, New York **1988**, pp. 191–192.
- [29] D. J. Green, P. Colombo, *MRS Bull.* **2003**, *28*, 296.
- [30] A. Füssel, D. Böttge, J. Adler, F. Marschallek, A. Michaelis, *Adv. Eng. Mater.* **2011**, *13*, 1008.
- [31] P. Colombo, J. Schmidt, G. Franchin, A. Zocca, J. Günster, *Am. Ceram. Soc. Bull.* **2017**, *96*, 16.
- [32] Z. C. Eckel, C. Zhou, J. H. Martin, A. J. Jacobsen, W. B. Carter, T. A. Schaedler, *Science* **2016**, *351*, 58.
- [33] T. A. Pham, D.-P. Kim, T.-W. Lim, S.-H. Park, D.-Y. Yang, K.-S. Lee, *Adv. Funct. Mater.* **2006**, *16*, 1235.
- [34] E. Zanchetta, M. Cattaldo, G. Franchin, M. Schwentenwein, J. Homa, G. Brusatin, P. Colombo, *Adv. Mater.* **2016**, *28*, 370.
- [35] Y. de Hazan, D. Penner, *J. Eur. Ceram. Soc.* **2017**, *37*, 5205.
- [36] Z. Fu, L. Schlier, N. Travitzky, P. Greil, *Mater. Sci. Eng. A* **2013**, *560*, 851.
- [37] A. Zocca, C. M. Gomes, A. Staude, E. Bernardo, J. Günster, P. Colombo, *J. Mater. Res.* **2013**, *28*, 2243.
- [38] H. Chen, X. Wang, F. Xue, Y. Huang, K. Zhou, D. Zhang, *J. Eur. Ceram. Soc.* **2018**, *38*, 5294.
- [39] G. Pierin, C. Grotta, P. Colombo, C. Mattevi, *J. Eur. Ceram. Soc.* **2016**, *36*, 1589.
- [40] J. W. Kemp, N. S. Hmeidat, B. G. Compton, *J. Am. Ceram. Soc.* **2020**, *103*, 4043.
- [41] G. Franchin, L. Wahl, P. Colombo, *J. Am. Ceram. Soc.* **2017**, *100*, 4397.
- [42] M. Mahmoudi, C. Wang, S. Moreno, S. R. Burlison, D. Alatalo, F. Hassanipour, S. E. Smith, M. Naraghi, M. Minary-Jolandan, *ACS Appl. Mater. Interfaces* **2020**, *12*, 31984.
- [43] A. Kulkarni, G. D. Sorarù, J. M. Pearce, *Addit. Manuf.* **2020**, *32*, 100988.
- [44] T. Friedel, N. Travitzky, F. Niebling, M. Scheffler, P. Greil, *J. Eur. Ceram. Soc.* **2005**, *25*, 193.
- [45] A. Bowyer, *3D Print. Addit. Manuf.* **2014**, *1*, 4.
- [46] Z. Lu, J. Cao, Z. Song, D. Li, B. Lu, *Virtual Phys. Prototyp.* **2019**, *14*, 333.
- [47] B. T. Wittbrodt, A. G. Glover, J. Laureto, G. C. Anzalone, D. Oppliger, J. L. Irwin, J. M. Pearce, *Mechatronics* **2013**, *23*, 713.
- [48] J. Kietzmann, L. Pitt, P. Berthon, *Bus. Horiz.* **2015**, *58*, 209.
- [49] P. Jana, O. Santoliquido, A. Ortona, P. Colombo, G. D. Sorarù, *J. Am. Ceram. Soc.* **2018**, *101*, 2732.
- [50] A. Frick, A. Rochman, *Polym. Test.* **2004**, *23*, 413.
- [51] G. D. Sorarù, G. D'Andrea, R. Campostrini, F. Babonneau, *J. Mater. Chem.* **1995**, *5*, 1363.
- [52] R. Chavez, E. Ionescu, C. Balan, C. Fasel, R. Riedel, *J. Appl. Polym. Sci.* **2011**, *119*, 794.
- [53] M. Herrera, G. Matuschek, A. Ketttrup, *Polym. Degrad. Stab.* **2002**, *78*, 323.
- [54] S. I. Andronenko, I. Stiharu, S. K. Misra, *J. Appl. Phys.* **2006**, *99*, 113907.
- [55] G. D. Sorarù, C. Tavonatti, L. Kundanati, N. Pugno, M. Biesuz, *J. Am. Ceram. Soc.* **2020**, *103*, 6519.
- [56] M. Narisawa, F. Funabiki, A. Iwase, F. Wakai, H. Hosono, *J. Am. Ceram. Soc.* **2015**, *98*, 3373.
- [57] L. David, R. Bhandavat, U. Barrera, G. Singh, *Nat. Commun.* **2016**, *7*, 10998.
- [58] E. Ionescu, S. Bernard, R. Lucas, P. Kroll, S. Ushakov, A. Navrotsky, R. Riedel, *Adv. Eng. Mater.* **2019**, *21*, 1900269.
- [59] H.-Y. Ryu, Q. Wang, R. Raj, *J. Am. Ceram. Soc.* **2010**, *93*, 1668.
- [60] F. Scheffler, P. Claus, S. Schimpf, M. Lucas, M. Scheffler, in *Cellular Ceramics*, John Wiley & Sons, Ltd, New York **2005**, pp. 454–483.
- [61] T. Fend, D. Trimis, R. Pitz-Paal, B. Hoffschmidt, O. Reutter, in *Cellular Ceramics*, John Wiley & Sons, Ltd, New York **2005**, pp. 342–360.
- [62] S. Gianella, D. Gaia, A. Ortona, *Adv. Eng. Mater.* **2012**, *14*, 1074.
- [63] A. Sommers, Q. Wang, X. Han, C. T'Joel, Y. Park, A. Jacobi, *Appl. Therm. Eng.* **2010**, *30*, 1277.
- [64] S. Modena, G. D. Sorarù, Y. Blum, R. Raj, *J. Am. Ceram. Soc.* **2005**, *88*, 339.
- [65] Z. L. Sun, Y. Zhou, D. C. Jia, X. M. Duan, Z. H. Yang, D. Ye, P. F. Zhang, Q. Zhang, *Mater. Lett.* **2012**, *72*, 57.
- [66] B. Santhosh, C. Vakifahmetoglu, E. Ionescu, A. Reitz, B. Albert, G. D. Sorarù, *Ceram. Int.* **2020**, *46*, 5594.
- [67] W. Zhang, C. Feng, G. Yang, G. Li, X. Ding, S. Wang, Y. Dou, Z. Zhang, J. Chang, C. Wu, X. Jiang, *Biomaterials* **2017**, *135*, 85.
- [68] C. Gao, Y. Deng, P. Feng, Z. Mao, P. Li, B. Yang, J. Deng, Y. Cao, C. Shuai, S. Peng, *Int. J. Mol. Sci.* **2014**, *15*, 4714.

- [69] S. Bose, S. Vahabzadeh, A. Bandyopadhyay, *Mater. Today* **2013**, *16*, 496.
- [70] P. Lagonegro, F. Rossi, C. Galli, A. Smerieri, R. Alinovi, S. Pinelli, T. Rimoldi, G. Attolini, G. Macaluso, C. Macaluso, S. E. Saddow, G. Salviati, *Mater. Sci. Eng. C* **2017**, *73*, 465.
- [71] R. Zhuo, P. Colombo, C. Pantano, E. A. Vogler, *Acta Biomater.* **2005**, *1*, 583.
- [72] B. Leukers, H. Gülkan, S. H. Irsen, S. Milz, C. Tille, H. Seitz, M. Schieker, *Mater. Werkst.* **2005**, *36*, 781.
- [73] Economic savings for scientific free and open source technology: A review – ScienceDirect, <https://www.sciencedirect.com/science/article/pii/S2468067220300481>.
- [74] A. Emelogu, M. Marufuzzaman, S. M. Thompson, N. Shamsaei, L. Bian, *Addit. Manuf.* **2016**, *11*, 97.
- [75] D. S. Thomas, S. W. Gilbert, **2014**, <https://nvlpubs.nist.gov/nistpubs/SpecialPublications/NIST.SP.1176.pdf>.
- [76] M. Kreiger, J. M. Pearce, *ACS Sustain. Chem. Eng.* **2013**, *1*, 1511.
- [77] G. Costabile, M. Fera, F. Fruggiero, A. Lambiase, D. Pham, *Int. J. Ind. Eng. Comput.* **2017**, 263.
- [78] J. Pearce, C. M. Blair, K. Laciak, R. Andrews, A. Nosrat, I. Zelenika-Zovko, *J. Sustain. Dev.* **2010**, *3*, p17.
- [79] G. D. Sorarù, L. Kundanati, B. Santhosh, N. Pugno, *J. Am. Ceram. Soc.* **2019**, *102*, 907.